Carbon 103 (2016) 172–180

Contents lists available at ScienceDirect

Carbon

journal homepage: www.elsevier.com/locate/carbon

Functionalized graphene oxide in microbial engineering: An effective stimulator for bacterial growth

Yinchan Luo [a], Xinxing Yang [b], Xiaofang Tan [a], Ligeng Xu [a, *], Zhuang Liu [a], Jie Xiao [b], Rui Peng [a, *]

[a] Institute of Functional Nano & Soft Materials (FUNSOM), Jiangsu Key Laboratory for Carbon-Based Functional Materials & Devices, Soochow University, 199 Ren'ai Rd., Suzhou, Jiangsu 215123, China
[b] Department of Biophysics and Biophysical Chemistry, Johns Hopkins University, School of Medicine, 725 N. Wolfe Street, WBSB 708, Baltimore, MD 21205, USA

ARTICLE INFO

Article history:
Received 7 October 2015
Received in revised form
2 March 2016
Accepted 3 March 2016
Available online 4 March 2016

ABSTRACT

Whether graphene and graphene oxide (GO) would affect the activities of bacteria has been under debate. Nevertheless, how graphene derivatives with biocompatible coatings interact with microorganisms and the underlying mechanisms are important issues for nanobiotechnology, and remain to be further explored. Herein, three new types of nano-GOs functionalized with polyethylene glycol (nGO-PEGs) were synthesized by varying the PEGylation degree, and their effects on *Escherichia coli* (*E. coli*) were carefully investigated. Interestingly, nGO-PEG (1:1), the one with relatively lower PEGylation degree, could significantly stimulate bacterial growth, whereas as-made GO and the other two nGO-PEGs showed no effect. Further analysis revealed that nGO-PEG (1:1) treatment significantly accelerated FtsZ-ring assembly, shortening Phase 1 in the bacterial cell cycle. Both DNA synthesis and extracellular polymeric substance (EPS) secretion were also dramatically increased. This unique phenomenon suggests promising potentials in microbial engineering as well as in clinical detection of bacterial pathogens. As a proof-of-concept, nGO-PEG (1:1) treatment could remarkably enhance (up to 6-fold) recombinant protein production in engineered bacteria cells. To our best knowledge, this is the first demonstration of functionalized GO as a novel, positive regulator in microbial engineering. Moreover, our work highlights the critical role of surface chemistry in modulating the interactions between nanomaterials and microorganisms.

1. Introduction

In recent years, graphene and its derivatives with many unique physicochemical properties have attracted tremendous attention in various fields. In the fields of biomedical research, there have been numerous reports demonstrating the use of graphene and its derivatives as biosensing platforms [1–7], bio-imaging probes [8–11], drug and gene delivery carriers [12–16], cancer therapy agents [17–21], protein modulators [22,23], antibacterial agents [24–27], as well as tissue engineering materials [28–30], achieving many exciting results in recent years. How graphene-based nanomaterials would interact with different biological systems has thus also been extensively investigated. It has been uncovered that raw graphene or graphene oxide (GO) without further modification usually would impose disturbances on biological systems such as dose-dependent or size-dependent toxicities, including genotoxicity, to cells or animals [27,31–34]. However, when graphene or GO is functionalized via appropriate surface modifications, their toxicity could be remarkably reduced. It is now generally accepted that the behaviors of graphene and GO in biological systems are closely related to the size and surface chemistry of those materials.

Recently, the interactions between graphene derivatives and microorganisms have also received substantial interests. Several previous studies have demonstrated that GO could be used to kill or inactivate bacteria via possible mechanisms including ROS generation, interaction of the sharp edges of GO sheets with bacterial cell wall and cell membrane to disrupt cell integrity, and wrapping bacteria with GO sheets to reduce their activities [25–27,35]. Moreover, Akhavan et al. reported that growth of bacteria on GO could in turn reduce GO to bactericidal graphene [36]. On the

* Corresponding authors.
E-mail addresses: lgxu@suda.edu.cn (L. Xu), rpeng@suda.edu.cn (R. Peng).

http://dx.doi.org/10.1016/j.carbon.2016.03.012
0008-6223/

contrary, a few reports have shown that GO was able to increase the growth or activity of certain bacteria [37–39]. In addition, little effect of bare GO on bacteria has been also reported [40,41]. Such differences in reported results may be due to the different experimental conditions (e.g. differences in the preparation of GO samples, the size variations and chemical states of GO samples, as well as culturing bacteria in the presence or absences of proteins). Although the interactions between as-made GO with bacteria have been explored, how nano-GO with biocompatible coatings such as polyethylene glycol (PEG) conjugation would affect the activities of microorganisms as well as the underlying mechanisms have been rarely studied. Such questions raise important issues for nanotechnology in microbiology, and therefore need further attention.

In this work, we newly developed a series of PEGylated nano-GOs (nGO-PEGs) and explored their interactions with genetically engineered strains of gram-negative bacteria *Escherichia coli* (*E. coli*), which have been extensively used in biological research, microbial engineering, and industry. Three types of nGO-PEGs with varying PEGylation degrees were synthesized by conjugation of GO with 10 kDa amine-terminated six-arm-branched PEG (10k-6*br*-PEG-NH_2) at different feeding GO:PEG ratios (GO:PEG = 1:1, 1:2.5, 1:5) using optimized procedure. Interestingly, nGO-PEG (1:1), the one with a relatively low level of PEGylation could greatly stimulate bacterial growth, while no obvious effect on cell viability was observed for either bare GO or nGO-PEGs with higher degrees of PEGylation. Further analysis showed that nGO-PEG (1:1) could significantly accelerate FtsZ-ring assembly process, shortening the first stage of the bacterial cell cycle. Both DNA synthesis and the secretion of extracellular polymeric substance (EPS) were dramatically increased by nGO-PEG (1:1) treatment. More importantly, we further demonstrated that nGO-PEG (1:1) could be utilized as a novel, positive regulator to remarkably enhance the recombinant protein production in bacteria, indicating its potential for further applications in microbial engineering.

2. Experimental

2.1. Materials and reagents

PEG (10k-6*br*-PEG-NH_2) was purchased from Sunbio Inc. (South Korea). All other reagents were purchased from Sigma–Aldrich (St. Louis, MO, USA).

2.2. Preparation and characterization of GO and PEGylated GO dispersions

GO was produced from graphite following a Hummers method with slight modifications [22,42]. Before PEGylation, 1.8 g NaOH was added into the 10 mL GO suspension (~1 mg/mL) and bath-sonicated for 4 h, then neutralized and purified by rinsing and filtration. Three types of PEGylated GO (feeding GO:PEG mass ratios = 1:1, 1:2.5, 1:5) were prepared by mixing 1 mg/mL GO dispersion with 1, 2.5, 5 mg/mL of PEG. Following 30 min bath sonication with the addition of 1 and 2 mg of N-(3-dimethylaminopropyl)-N-ethylcarbodiimide hydrochloride (EDC) at 5 and 25 min, respectively, the solutions were stirred at room temperature for overnight. Excess PEG and other reagents were removed by ultra-filtration through 100 kDa molecular-weight cut-off (MWCO) centrifugal filters.

Both as-made GO and nGO-PEGs were characterized by atomic force microscope (AFM) analysis using a MutiMode V AFM (Veeco), Fourier transform infrared spectroscopy (FT-IR) using a Hyperion series FT-IR spectrometer (Bruker), and Dynamic light scattering (DLS) on a Zen3690 (Malvern) at the scattering angle $\theta = 17°$. The concentrations of GO and nGO-PEGs were calculated using their absorbance at 230 nm recorded using a UV–vis spectrometer (mass extinction coefficient of 65 mg mL^{-1} cm^{-1}) [22]. The PEG contents in nGO-PEG (1:1), nGO-PEG (1:2.5), and nGO-PEG (1:5), were estimated to be 38.6%, 55.7%, and 60.8% respectively, using thermogravimetric analysis (TGA, Supporting Information Fig. S1) as previously reported [13].

The chemical states of nGO-PEG (1:1) were characterized using X-ray photoelectron spectroscopy (XPS). nGO-PEG (1:1) nanosheets exposed to *E. coli* cells in liquid Luria-Bertan (LB) medium (or incubated in liquid LB medium without the presence of bacteria as control) at 37 °C in the shaking incubator were separated and washed three times with 1 × PBS, and then characterized using XPS with a monochromatic Al *Kα* source in ultra-high vacuum ($<10^{-7}$ Pa). The XPS peaks were deconvoluted by using Gaussian components after a Shirley background subtraction.

2.3. Bacterial culture

E. coli cells (DH5α and BL21 (DE3)-pLysS) were cultured in liquid LB medium in a shaking incubator at 37 °C overnight. The overnight culture was then re-inoculated (1:100) into fresh LB medium and grown at 37 °C for 2–3 h till an optical density at 600 nm (OD_{600}) of 0.5 was reached, bringing the bacterial cells into log phase.

2.4. Bacterial viability assay

Log phase *E. coli* cells were inoculated 1:10 in fresh LB medium containing 1 × PBS or different nanomaterials as indicated in the text, and grown for 2.5 h at 37 °C in the shaking incubator. The cultures were then diluted and dispensed in 96-well plates. For each culture, a well with LB medium containing the same amount of nanomaterials but no *E. coli* cells was set as the blank, and the metabolic activities of bacterial cells in these cultures were analyzed using the colorimetric 3-(4,5-dimethylthiazol-2-yl)-2,5-diphenyl tetrazolium bromide (MTT) assay as described [40]. All measurements were carried out in triplicate or quadruplicate.

Colony forming units (CFU) counting method was used to analyze the numbers of viable bacterial cells in the above cultures. Briefly, gradient dilutions of each culture were plated on LB-agar plates in triplicate, followed by incubating at 37 °C for 16 h, and the bacterial colonies formed were counted and photographed.

2.5. Time-lapse photography of bacterial growth and division

Time-lapse photography of bacterial growth and division was carried out following a previous protocol [40,43] with modifications. Briefly, 1 mm-thick LB-agar pads with a flat, smooth surface were prepared by plating 70 μL LB medium containing 3% (w/v) agar between two clean round coverslips. Individual nGO-PEG (1:1) treated *E. coli* cells (DH5α) were sandwiched between a glass bottom cell culture dish and the LB-agar pad containing 20 μg/mL nGO-PEG (1:1). Untreated *E. coli* cells were sandwiched using normal LB-agar pad as control. The bacteria growth was monitored and imaged using the confocal microscope (Leica TCS SP5) every 5 min while incubating at 37 °C in the temperature-control accessory.

For real-time monitoring of FtsZ-ring dynamics and bacterial cell cycle, DH5α cells were transformed with pCA24N-FtsZ-GFP, a plasmid encoding a fusion of green fluorescent protein (GFP) to the essential bacterial cell division protein FtsZ (FtsZ-GFP). The log phase DH5α cells carrying pCA24N-FtsZ-GFP were induced by isopropyl β-D-1-thiogalactopyranoside (IPTG; final concentration 1 μM) for 15 min allowing proper expression of FtsZ-GFP, and then re-inoculated (1:100) into fresh LB with or without 20 μg/mL nGO-PEG (1:1) (37 °C, 2 h) before sandwiching on LB-agar pads for

imaging. For better imaging of the FtsZ-GFP, normal LB-agar pads were used for both the control group and the nGO-PEG (1:1) treated group.

2.6. DNA synthesis analysis

Bacterial DNA synthesis was analyzed by 5-ethynyl-2'-deoxyuridine (EdU) labeling method using Click-iT EdU Alexa Fluor Imaging Kit (Ruibo, Guang Dong, China) according to the manufacturer's protocol. *E. coli* cells (DH5α) were labeled with 1 μM EdU for 30 min, and the EdU incorporation was analyzed by a flow cytometer (BD). The relative EdU incorporation was calculated using the formula: $\triangle EdU_{incorporation} = (I_T - I_o)/(I_C - I_o)$ *100%, where I_0: blank, i.e. mean fluorescence intensity (MFI) of unlabeled cells; I_C: MFI of control cells; I_T: MFI of nGO-PEG (1:1) treated cells.

2.7. Morphological characterization of E. coli

E. coli cells (DH5α) were collected, washed twice with 1 × PBS, and then fixed with 2.5% glutaraldehyde solution for 2 h. The samples were dehydrated with sequential treatment of 50, 70, 85, 90, and 100% ethanol for 10 min, gold sputter-coated, and imaged using a scanning electronic microscope (SEM, Quanta 200FEG, FEI) [44].

2.8. EPS extraction and quantification

EPS on *E. coli* cell (DH5α) surface were extracted following a formaldehyde-NaOH method [45]. The EPS polysaccharide content was quantitated by Phenol-sulfuric acid method using glucose as the standard [46]. The EPS protein content was measured by the Bradford assay using bovine serum albumin as the standard [47].

2.9. Recombinant protein production

Expression of recombinant FtsZ-GFP in DH5α cells carrying the high-copy plasmid pCA24N-FtsZ-GFP (T5-lac promoter) was induced by addition of IPTG to a final concentration of 1 μM for 1 h. Expression of recombinant GFP in BL21 (DE3)-pLysS cells carrying the low-copy plasmid pET28a-GFP (T7-lac promoter) was induced by addition of IPTG to a final concentration of 2 μM for 1 h. GFP fluorescence was measured by flow cytometry.

2.10. Cell viability assay of mammalian cells

Raw cells and NIH3T3 cells were cultured in Dulbecco's modified Eagle's medium (DMEM) supplemented with 10% fetal bovine serum at 37 °C. Both types of cells were treated with indicated concentrations of nGO-PEG (1:1) at 37 °C for 24 h. Their viabilities were measured using MTT assay following the standard protocol.

3. Results and discussion

3.1. Preparation and characterization of functionalized GO nanosheets

GO nanosheets were made from graphite by using an improved Hummer's method [42]. 10k-6*br*-PEG-NH_2 was conjugated to the carboxyl groups on GO nanosheets via amide formation at different feeding weight ratios (GO:PEG = 1:1, 1:2.5, 1:5) to prepare nGO-PEG (1:1), nGO-PEG (1:2.5), and nGO-PEG (1:5), respectively. As revealed by AFM images (Fig. 1a), as-made GO nanosheets were mostly single-layered with thickness of around 1 nm. After PEGylation, the thickness of nGO-PEG (1:1), nGO-PEG (1:2.5), and nGO-PEG (1:5) increased to around 2 nm, 2.5 nm, and 3 nm, respectively, correlated with increasing levels of PEGylation on the GO surface. The sheet sizes of these PEGylated GO nanosheets (20–40 nm) were much smaller than that of as-made GO before PEGylation, which should be attributed to the sonication during the PEGylation step. PEGylation of GO was also demonstrated by FT-IR spectra (Supporting Information Fig. S2) and zeta potential (Fig. 1b). As expected, owing to the amino groups on the 10k-6*br*-PEG-NH_2 polymer conjugated to GO, the zeta potentials of those samples shifted from −40.1 mV for as-made GO, to −26.5 mV, −20.2 mV, and −16.5 mV, for nGO-PEG (1:1), nGO-PEG (1:2.5), and nGO-PEG (1:5), respectively (Fig. 1b). As shown in Fig. 1c, as-made GO, although well dispersed in water, would aggregate in LB medium in the presence of salts, whereas no noticeable aggregation was observed for the three nGO-PEG samples under the same conditions. This demonstrates that, even at the relatively low PEGylation level (i.e. feeding weight ratio GO:PEG = 1:1), PEGylation could greatly improve the dispersibility of those nanosheets in physiological solutions.

3.2. Surface chemistry-dependent stimulation of bacterial growth by PEGylated GO

The effects of as-made GO and the three types of nGO-PEG on *E. coli* cell viability were firstly analyzed using the MTT method. As shown in Fig. 2a, without PEGylation, as-made GO showed barely any effect on *E. coli* cell viability, consistent with our previous reports [40,41]. The two nGO-PEGs with higher levels of PEGylation, nGO-PEG (1:2.5) and nGO-PEG (1:5), as well as PEG polymer by itself, also showed no effect on the viability of *E. coli* (Fig. 2a). Interestingly, nGO-PEG (1:1) with the relatively low level of PEGylation (feeding weight ratio GO:PEG = 1:1) strongly increased *E. coli* viability to around 180% at the concentration of 20 μg/mL. The growth stimulating effect of nGO-PEG (1:1) was also confirmed by CFU counting method (Fig. 2b and c). Consistent with the results from the MTT assay, nGO-PEG (1:1) treatment could increase the growth of bacteria in a dose-dependent manner (Fig. 2b).

Such surface chemistry-dependent stimulation effect on bacterial growth is intriguing. Unlike the previous report regarding the interaction of *E. coli* with GO could lead to reduction of GO [36], exposure of nGO-PEG (1:1) to *E. coli* cells barely changed its O/C ratio (Supporting Information Fig. S3), suggesting that the interaction between *E. coli* cells and nGO-PEG (1:1) might be different from the interaction of *E. coli* cells with GO. Therefore, it is possible that nGO-PEG (1:1) with a low PEG density on its surface may provide a unique nano-bio interface between the nanomaterial and the bacteria, and then affect the growth of bacteria via certain mechanism(s). Higher levels of PEGylation may make nGO to be too inert and abolish its interaction with bacteria. The detailed mechanism(s) are still not fully understood. Nevertheless, we further carefully investigated how nGO-PEG (1:1) would affect the bacteria growth.

3.3. Significant shortening of the bacterial growth cycle by nGO-PEG(1:1)

To further analyze the growth stimulating effect of nGO-PEG (1:1), the real-time growth of *E. coli* cells were monitored. The dilute suspensions of the *E. coli* culture after growth in liquid LB medium with or without nGO-PEG (1:1) for 2 h were plated on corresponding LB agar plates, and the cell growth were monitored under a light microscope. In the presence of nGO-PEG (1:1), *E. coli* cells grew much faster than the control did (Fig. 3), and the bacterial doubling times (on LB agar plates) were calculated to be 43 min and 75 min for nGO-PEG (1:1)-treated cells and the untreated ones, respectively.

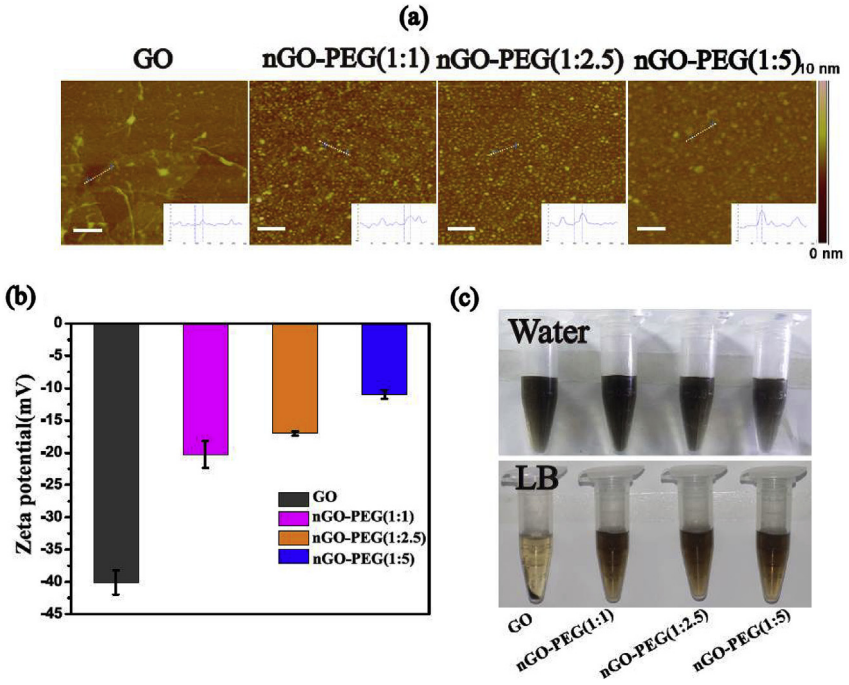

Fig. 1. Characterization of GO and nGO-PEG nanosheets used in the study: AFM images and the corresponding depth profiles (a), Zeta potential (b), and dispersibilities in water and LB medium (c) of GO, nGO-PEG (1:1), nGO-PEG (1:2.5), and nGO-PEG (1:5). Photos in (c) were taken after the solutions (20 μg/mL) were centrifuged at 21,000 g for 5 min. Scare bar in (a) = 200 nm. (A color version of this figure can be viewed online.)

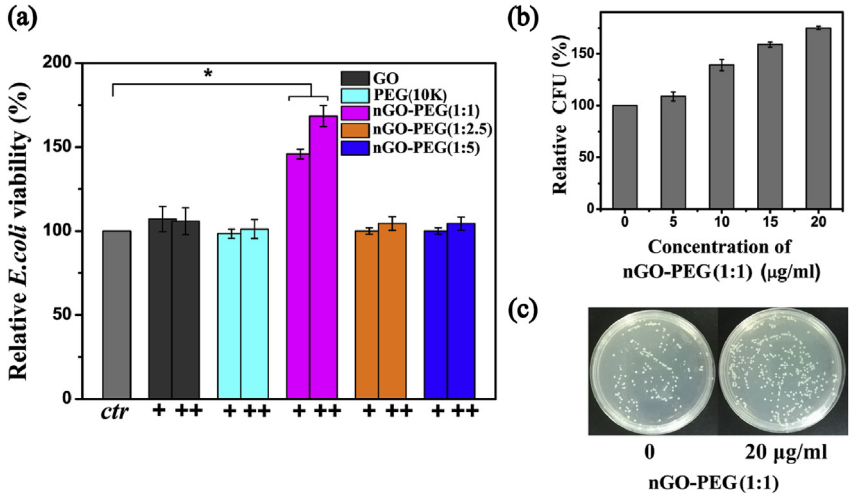

Fig. 2. Effects of GO nanosheets with different surface modifications on bacterial growth. (a) *E. coli* cells were grew in liquid LB medium with either as-made GO, different nGO-PEG nanosheets, or the corresponding PEG polymer for 2.5 h. Cells grew in normal liquid LB medium were used as control (ctr). Their viabilities were analyzed using the MTT method. + and ++ represent 10 and 20 μg/mL (b) CFU counting of viable bacteria in the cultures after being treated with indicated concentrations of nGO-PEG (1:1) at 37 °C for 2.5 h. Representing photographs of bacterial colonies formed on LB-agar plates are shown in (c). Error bars represent the standard deviations ($n \geq 3$). *$P < 0.05$. (A color version of this figure can be viewed online.)

Given the dramatic shortening of the bacterial doubling time upon nGO-PEG (1:1) treatment, one question arises as to whether the entire cell growth cycle is shortened proportionally, or only part(s) of the cell growth cycle are affected. To address this question, *E. coli* cells expressing a fusion of GFP to the essential bacterial cell division protein FtsZ (FtsZ-GFP) were used [43]. At the future site of the septum of bacterial cell division, FtsZ protein assemble to a ring-like structure, also called FtsZ-ring or Z-ring, which is essential for bacterial cell division [48], and the GFP-tag allows us to closely monitor the dynamics of FtsZ protein and FtsZ-ring. As shown in Fig. 4a and b, according to the dynamics of FtsZ-ring, the cell cycle of *E. coli* could be divided into three major phases: Phase 1 (P1), Phase 2 (P2), and Phase 3 (P3). P1 is the first stage, during which FtsZ protein assembles into a ring structure at mid-cell (Fig. 4a and b, I-II). During this phase, the bacterium replicates its DNA and synthesizes proteins, preparing for subsequent steps. P2 is the process of maturation of the septum and FtsZ-ring (Fig. 4a and b, II-III, see the septum marked by a white arrow in III). FtsZ maintains the dynamic ring structure during P2 and recruits downstream proteins for the division machinery. P3 is the last stage

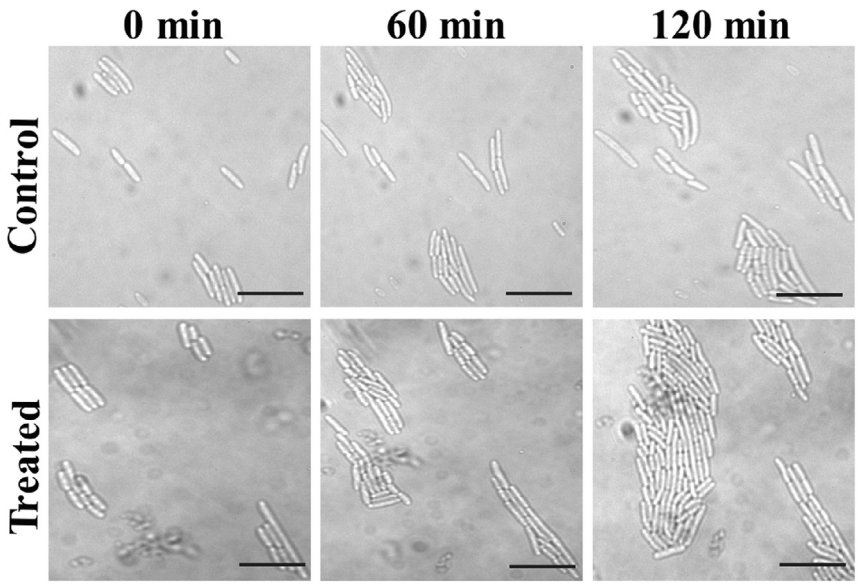

Fig. 3. Real-time bacterial growth of *E. coli* cells. **Control**: *E. coli* cells were grew in normal liquid LB medium for 2 h, the culture was then diluted and plated on normal LB-agar pad; **Treated**: *E. coli* cells were grew in liquid LB medium with 20 μg/mL nGO-PEG (1:1) for 2 h, then diluted and plated on LB-agar pad containing 20 μg/mL nGO-PEG (1:1). The bacterial growth was monitored under a light microscope and imaged. Scale bar: 5 μm.

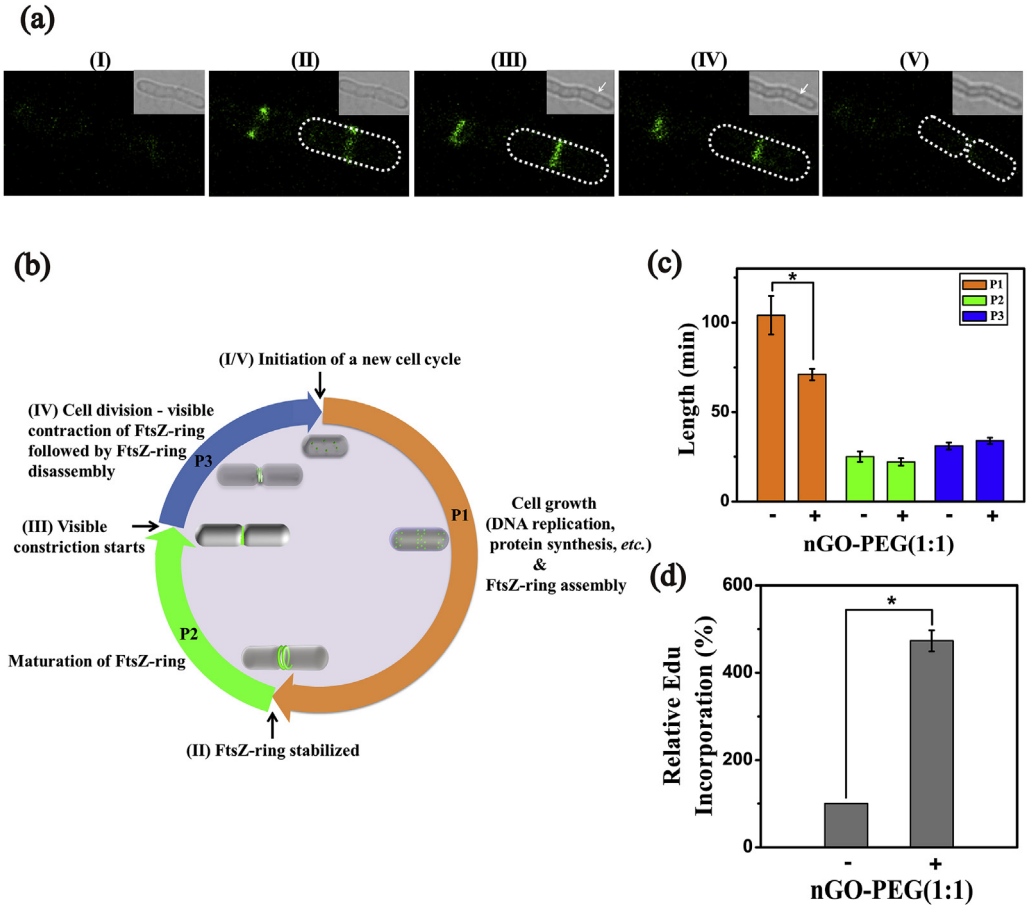

Fig. 4. Shortening of the bacterial growth cycle after nGO-PEG (1:1) treatment. Live cell fluorescence imaging (a) and a scheme (b) showing the dynamics of FtsZ-ring in a full cell cycle of *E. coli* cells expressing FtsZ-GFP (green). The bacterial cell wall is demonstrated by a dashed line. The corresponding bright-field images were displayed at the up-right corners in (a), with the septum of bacterial cell division marked by a white arrow. (I)/(V): Cell division completes and a new cell cycle starts; (II): FtsZ-ring stabilizes at mid-cell; (III) Visible constriction of FtsZ-ring starts; (IV): FtsZ-ring contracts, then disassembles, concluded by cell separation. P1: Phase 1; P2: Phase 2; P3: Phase 3. (c) After *E. coli* cells being treated with or without 20 μg/mL nGO-PEG (1:1) for 2.5 h, the length of each phase in the cell cycle were analyzed according to the dynamics of FtsZ-ring as shown in (a & b). Error bars represent the standard deviations (n = 20, $^*P < 0.05$). (d) Incorporation of EdU into newly synthesized DNA in *E. coli* cells with or without 20 μg/mL nGO-PEG (1:1) treatment was analyzed by flow cytometry. Error bars represent the standard deviations (n = 3, $^*P < 0.01$). (A color version of this figure can be viewed online.)

of the cell division cycle, in which FtsZ-ring contracts, and then disassembles, concluded by daughter cell separation (Fig. 4a and b, III-V). As shown in Fig. 4c, compared with untreated bacteria, *E. coli* cells treated with nGO-PEG (1:1) showed substantially shortened P1, whereas the other two phases P2 & P3 appeared unaffected, suggesting that nGO-PEG (1:1) could affect the bacterial growth cycle by expediting Z-ring assembly and therefore shortening the first stage (P1), which is the preparation stage for later steps of cell division.

Since one of the major events happen in P1 other than Z-ring assembly is DNA replication, the effect of nGO-PEG (1:1) on new DNA synthesis was investigated using a thymidine analog EdU [49]. As shown in Fig. 4d, in *E. coli* cells treated with nGO-PEG (1:1), the incorporation of EdU in newly synthesized bacterial DNA increased to nearly 5 fold of that in untreated cells, suggesting that the bacterial DNA synthesis could be greatly promoted by nGO-PEG (1:1), consistent with the above findings showing shortened P1 in the *E. coli* cell cycle (Fig. 4c).

3.4. Effects of nGO-PEG(1:1) on E. coli cell surface and EPS secretion

During bacterial growth, aside from DNA replication, cells also synthesize large amount of macromolecules such as proteins, nucleic acids, phospholipids, and polysaccharides. A portion of these macromolecules are secreted to the environment as EPS, either forming a layer of high-molecular weight compounds on the cell outer surface, or being secreted to the growth medium [50,51]. To analyze the possible effect of nGO-PEG (1:1) on *E. coli* cell surface, cells were grew in liquid LB medium with or without nGO-PEG (1:1), and then imaged using SEM. As shown in Figure 5a–5d, although both groups of bacteria were typically rod-shaped with smooth and intact cell walls, compared with untreated cells, a thicker layer of substance on the cell surface and increased cell–cell adhesion could be observed for cells treated with nGO-PEG (1:1).

The EPS on the bacterial cell surface was also extracted and its main components were quantified. As shown in Fig. 5e, nGO-PEG (1:1) treatment resulted in over 2- and 3-fold increase for polysaccharide content and protein content, respectively, giving an increase of 2.6-fold for total EPS content, demonstrating largely elevated EPS production and secretion, consistent with the SEM data. EPS can provide the matrix to support extracellular enzymes in aquatic systems, protecting their activity and preventing them from diffusing into the growth medium [51]. Given the critical role of extracellular enzymes, which are essential for the decomposition of organic nutrients in bacterial growth [50], the thickened EPS layer on the nGO-PEG (1:1)-treated cell surface might generate a more friendly microenvironment to facilitate cell growth.

3.5. Promising potential of nGO-PEG(1:1) in microbial engineering

The development of DNA recombination techniques since late 1970s enabled production of proteins of interests in host cells at all scales [52]. Since then, recombinant protein production has become more and more critical for both biomedical research and industry, especially for pharmaceutical industry [53]. One of the important roles of *E. coli* in microbial engineering is the extensive use of genetically engineered *E. coli* cells as popular bacterial hosts for the production of recombinant proteins [54,55]. The results above have successfully demonstrated that nGO-PEG (1:1) could greatly stimulate the growth of bacteria. This is a novel application of functionalized GO in microbial engineering and could be used to promote recombinant protein synthesis.

As a proof-of-concept experiment, expression levels of recombinant proteins under the influence of nGO-PEG (1:1) were investigated using two examples. The first example was the *E. coli* cells used in the bacterial cell cycle analysis above, i.e. the DH5α cells carrying a high-copy plasmid encoding FtsZ-GFP. As shown in Fig. 6, under the same induction condition, compared with untreated cells, the treatment of 20 μg/ml nGO-PEG (1:1) led to over 6-fold increase in GFP fluorescence. Since the expression of recombinant proteins may vary when using different hosts, expression vectors, induction conditions, *etc.*, we also applied the nGO-PEG (1:1) treatment to another *E. coli* expression system as the second example: BL21 (DE3)-pLysS [56,57], a genetically engineered *E. coli* strain commonly used for protein expression, as the host; and pET28a [56,58], a general expression vector (low-copy plasmid), encoding GFP as the reporter. In this example, under the induction condition we used, GFP was expressed at a much lower level (about 30%, data not shown) to that in the first example. Similar to DH5α cells, the growth of BL21 (DE3)-pLysS cells could be stimulated by

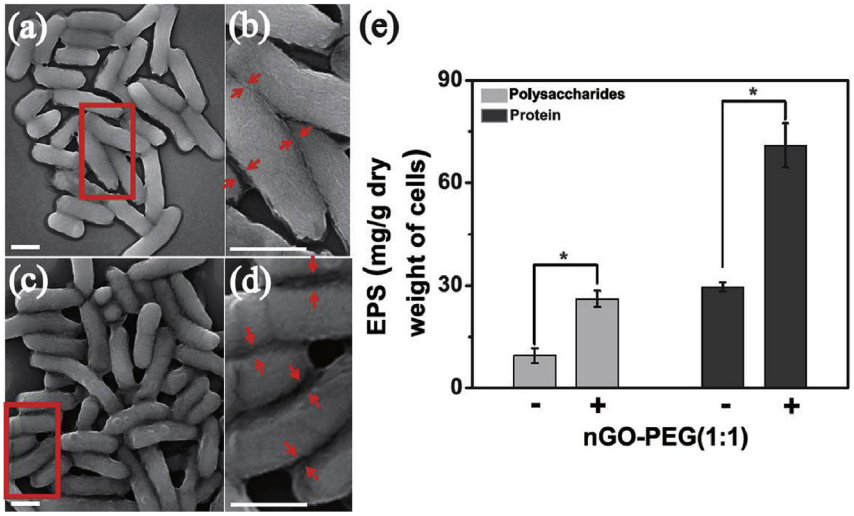

Fig. 5. Effect of nGO-PEG (1:1) on EPS secretion. (a–d) SEM images of *E. coli* cells without (a & b) and with (c & d) nGO-PEG (1:1) treatment. (b) and (d) are the magnified images of the red rectangles in (a) and (c), respectively. Scale bar: 500 nm. Pairs of arrows indicate the outer surfaces of two adjacent *E. coli* cells, and a clear layer of substance can be seen in-between the arrows in (d). (e) EPS on the bacterial cell surface was extracted, and the contents of polysaccharides and proteins were quantified. Error bars represent the standard deviations (n = 3, $^*P < 0.05$). (A color version of this figure can be viewed online.)

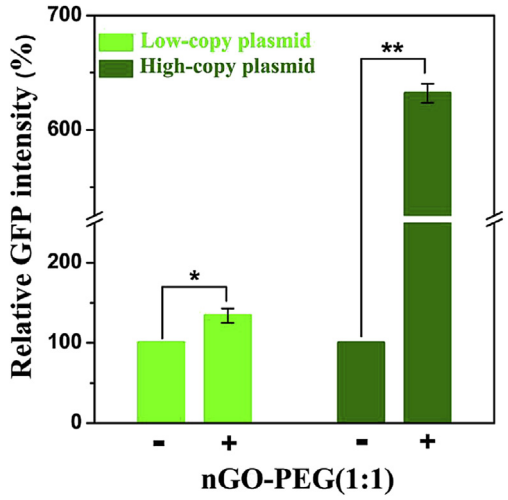

Fig. 6. Significant increase in recombinant protein production upon nGO-PEG (1:1) treatment. *E. coli* cells carrying either a low-copy plasmid or a high-copy plasmid encoding recombinant GFP constructs were grew in liquid LB medium with or without 20 μg/mL nGO-PEG (1:1) followed by IPTG induction. Expression level of GFP was recorded. Error bars represent the standard deviations (n = 3, $^{*}P < 0.05$, $^{**}P < 0.01$). (A color version of this figure can be viewed online.)

nGO-PEG (1:1) as well (Supporting Information Fig. S4). As shown in Fig. 6, in this low-protein-yield example, nGO-PEG (1:1) treatment was still able to increase GFP expression to about 1.3-fold. Both examples demonstrated the ability of nGO-PEG (1:1) in enhancing recombinant protein production in *E. coli* hosts. Given the important applications of recombinant proteins in biological research and industry, and the demands for higher protein yield, this functionalized GO nanosheets, nGO-PEG (1:1), might be particularly promising in microbial engineering, for example, as an efficient positive regulator for recombinant protein production.

3.6. Effect of nGO-PEG(1:1) on mammalian cells

Since nGO-PEG (1:1) can effectively stimulate the growth of bacteria, which are prokaryotic cells, we further analyzed whether it would affect the growth of eukaryotic cells. Two commonly used cell lines, mouse embryonic fibroblast (NIH3T3) and mouse mononuclear macrophage (RAW264.7) were used in the study. As shown in Fig. 7, for both RAW264.7 cells and NIH3T3 cells, after being treated with nGO-PEG (1:1) for 24 h at concentrations comparable to those used in the *E. coli* study (10–30 μg/mL), only about 10% increase in cell growth could be detected. Further increasing of the nGO-PEG (1:1) concentration (up to 100 μg/mL) could not promote cell growth, but rather resulted in certain levels of cytotoxicity towards both cells. The observed cytotoxicity of nGO-PEG (1:1) was slightly higher than those from previous similar reports [59,60], likely due to its lower level of functionalization on GO surface, which might be less sufficient to reduce the cytotoxicity of GO.

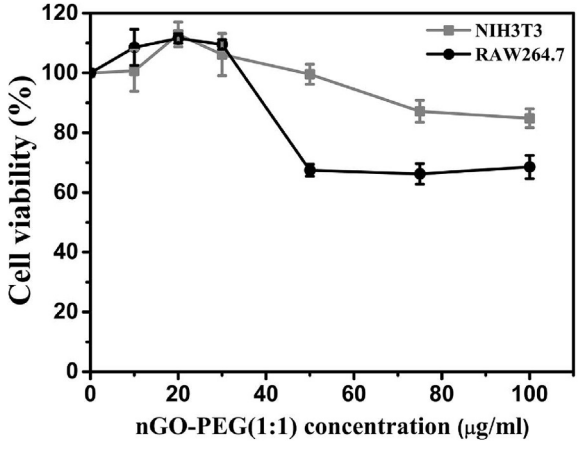

Fig. 7. Effects of nGO-PEG (1:1) on viabilities of mammalian cells. NIH3T3 and RAW264.7 cells were treated with increasing concentrations of nGO-PEG (1:1) for 24 h, and cell viabilities were analyzed using MTT method. Error bars represent the standard deviations (n = 3).

4. Conclusion

In summary, three new types of PEGlyated GO nanosheets with different levels of PEGylation were synthesized and their effects on *E. coli* cells were carefully investigated. While bare GO and nGO-PEGs with higher degrees of PEGylation exerted no appreciable effect on the growth and viabilities of bacteria within our tested dose range, nGO-PEG (1:1) with a relatively low PEGylation level showed a rather robust stimulating effect on bacterial growth. Further analysis revealed that such a unique growth-stimulating effect of nGO-PEG (1:1) was associated with shortened P1 phase in the bacterial cell cycle, during which significantly accelerated FtsZ-ring assembly and DNA synthesis were detected. 2–3 fold increase in EPS production was also revealed. As a proof-of-concept, we further applied nGO-PEG (1:1) as a positive regulator in microbial engineering, and demonstrated that the production of recombinant proteins from bacterial hosts could be significantly enhanced (up to 6-fold) upon treatment with nGO-PEG (1:1). Although future work is required to further investigate the mechanism underlying the stimulation of bacterial growth and any potential genotoxicity towards bacteria which might associate with the stimulated growth and DNA synthesis, our work reveals that the interactions between nanomaterials and microorganisms could be closely associated with and regulated through their surface chemistry and the nano-bio interfaces. In this case, specific PEGylation on the GO surface could generate a unique interface for interacting with bacteria. Nevertheless, this is to our best knowledge the first report of functionalized GO as a novel, positive regulator for bacterial growth, indicating its promising potentials in microbial engineering as well as in clinical detection of bacterial pathogens.

Acknowledgments

We thank Dr. Rosamund Daw for useful comments and suggestions. *E. coli* cells carrying the pET28a-GFP construct was a kind gift from Prof. Aoneng Cao (Shanghai University). This work is supported by the National Basic Research Program of China (973 Program, 2012CB932601 and 2011CB911000), NSFC (51132006, 31300824, and 51222203), China Postdoctoral Science Foundation (2013M530267), a project funded by the Priority Academic Program Development of Jiangsu Higher Education Institutions (PAPD), and Collaborative Innovation Center of Suzhou Nano Science and Technology.

Appendix A. Supplementary data

Supplementary data related to this article can be found at http://dx.doi.org/10.1016/j.carbon.2016.03.012.

References

[1] B.E.F. de Avila, E. Araque, S. Campuzano, M. Pedrero, B. Dalkiran, R. Barderas, R. Villalonga, E. Kilic, J.M. Pingarron, Dual functional graphene derivative-based electrochemical platforms for detection of the tp53 gene with single nucleotide polymorphism selectivity in biological samples, Anal. Chem. 87 (4) (2015) 2290–2298.

[2] M. Liu, J.P. Song, S.M. Shuang, C. Dong, J.D. Brennan, Y.F. Li, A graphene-based biosensing platform based on the release of dna probes and rolling circle amplification, ACS Nano 8 (6) (2014) 5564–5573.

[3] M. Yi, S. Yang, Z.Y. Peng, C.H. Liu, J.S. Li, W.W. Zhong, R.H. Yang, W.H. Tan, Two-photon graphene oxide/aptamer nanosensing conjugate for in vitro or in vivo molecular probing, Anal. Chem. 86 (7) (2014) 3548–3554.

[4] P.K. Ang, A. Li, M. Jaiswal, Y. Wang, H.W. Hou, J.T.L. Thong, C.T. Lim, K.P. Loh, Flow sensing of single cell by graphene transistor in a microfluidic channel, Nano Lett. 11 (12) (2011) 5240–5246.

[5] B.W. Zhu, Z.Q. Niu, H. Wang, W.R. Leow, H. Wang, Y.G. Li, L.Y. Zheng, J. Wei, F.W. Huo, X.D. Chen, Microstructured graphene arrays for highly sensitive flexible tactile sensors, Small 10 (18) (2014) 3625–3631.

[6] X.W. Wang, G.Z. Sun, P. Routh, D.H. Kim, W. Huang, P. Chen, Heteroatom-doped graphene materials: syntheses, properties and applications, Chem. Soc. Rev. 43 (20) (2014) 7067–7098.

[7] Q.Y. He, H.G. Sudibya, Z.Y. Yin, S.X. Wu, H. Li, F. Boey, W. Huang, P. Chen, H. Zhang, Centimeter-long and large-scale micropatterns of reduced graphene oxide films: fabrication and sensing applications, ACS Nano 4 (6) (2010) 3201–3208.

[8] Y. Zhang, T.R. Nayak, H. Hong, W.B. Cai, Graphene: a versatile nanoplatform for biomedical applications, Nanoscale 4 (13) (2012) 3833–3842.

[9] S.K. Pal, Versatile photoluminescence from graphene and its derivatives, Carbon 88 (2015) 86–112.

[10] V. Urbanova, K. Hola, A.B. Bourlinos, K. Cepe, A. Ambrosi, A.H. Loo, M. Pumera, F. Karlicky, M. Otyepka, R. Zboril, Thiofluorographene-hydrophilic graphene derivative with semiconducting and genosensing properties, Adv. Mater. 27 (14) (2015) 2305–2310.

[11] Z.T. Fan, S.H. Li, F.L. Yuan, L.Z. Fan, Fluorescent graphene quantum dots for biosensing and bioimaging, RSC Adv. 5 (25) (2015) 19773–19789.

[12] L.M. Zhang, J.G. Xia, Q.H. Zhao, L.W. Liu, Z.J. Zhang, Functional graphene oxide as a nanocarrier for controlled loading and targeted delivery of mixed anticancer drugs, Small 6 (4) (2010) 537–544.

[13] J. Zhang, L.Z. Feng, X.F. Tan, X.Z. Shi, L.G. Xu, Z. Liu, R. Peng, Dual-polymer-functionalized nanoscale graphene oxide as a highly effective gene transfection agent for insect cells with cell-type-dependent cellular uptake mechanisms, Part. Part. Syst. Char 30 (9) (2013) 794–803.

[14] H.Q. Dong, C.Y. Dong, T.B. Ren, Y.Y. Li, D.L. Shi, Surface-engineered graphene-based nanomaterials for drug delivery, J. Biomed. Nanotechnol. 10 (9) (2014) 2086–2106.

[15] L.M. Zhang, Z.X. Lu, Q.H. Zhao, J. Huang, H. Shen, Z.J. Zhang, Enhanced chemotherapy efficacy by sequential delivery of sirna and anticancer drugs using pei-grafted graphene oxide, Small 7 (4) (2011) 460–464.

[16] M.X. Zhang, Y.H. Cao, Y. Chong, Y.F. Ma, H.L. Zhang, Z.W. Deng, C.H. Hu, Z.J. Zhang, Graphene oxide based theranostic platform for T-1-weighted magnetic resonance imaging and drug delivery, ACS Appl. Mater. Interfaces 5 (24) (2013) 13325–13332.

[17] J.T. Robinson, S.M. Tabakman, Y.Y. Liang, H.L. Wang, H.S. Casalongue, D. Vinh, H.J. Dai, Ultrasmall reduced graphene oxide with high near-infrared absorbance for photothermal therapy, J. Am. Chem. Soc. 133 (17) (2011) 6825–6831.

[18] L.Y. Feng, L. Wu, X.G. Qu, New horizons for diagnostics and therapeutic applications of graphene and graphene oxide, Adv. Mater. 25 (2) (2013) 168–186.

[19] L.Y. Feng, Y. Chen, J.S. Ren, X.G. Qu, A graphene functionalized electrochemical aptasensor for selective label-free detection of cancer cells, Biomaterials 32 (11) (2011) 2930–2937.

[20] H. Zhang, H.X. Wu, J. Wang, Y. Yang, D.M. Wu, Y.J. Zhang, Y. Zhang, Z.G. Zhou, S.P. Yang, Graphene oxide-BaGdF5 nanocomposites for multi-modal imaging and photothermal therapy, Biomaterials 42 (2015) 66–77.

[21] L.Y. Yang, Y.T. Tseng, G.L. Suo, L.L. Chen, J.T. Yu, W.J. Chiu, C.C. Huang, C.H. Lin, Photothermal therapeutic response of cancer cells to aptamer-gold nanoparticle-hybridized graphene oxide under nir illumination, ACS Appl. Mater. Interfaces 7 (9) (2015) 5097–5106.

[22] L.L. Jin, K. Yang, K. Yao, S. Zhang, H.Q. Tao, S.T. Lee, Z. Liu, R. Peng, Functionalized graphene oxide in enzyme engineering: a selective modulator for enzyme activity and thermostability, ACS Nano 6 (6) (2012) 4864–4875.

[23] X.F. Tan, L.Z. Feng, J. Zhang, K. Yang, S. Zhang, Z. Liu, R. Peng, Functionalization of graphene oxide generates a unique interface for selective serum protein interactions, ACS Appl. Mater. Interfaces 5 (4) (2013) 1370–1377.

[24] S.Y. Yin, Y. Goldovsky, M. Herzberg, L. Liu, H. Sun, Y.Y. Zhang, F.B. Meng, X.B. Cao, D.D. Sun, H.Y. Chen, A. Kushmaro, X.D. Chen, Functional free-standing graphene honeycomb films, Adv. Funct. Mater. 23 (23) (2013) 2972–2978.

[25] Y.S. Tu, M. Lv, P. Xiu, T. Huynh, M. Zhang, M. Castelli, Z.R. Liu, Q. Huang, C.H. Fan, H.P. Fang, R.H. Zhou, Destructive extraction of phospholipids from Escherichia coli membranes by graphene nanosheets, Nat. Nanotechnol. 8 (8) (2013) 594–601.

[26] O. Akhavan, E. Ghaderi, Toxicity of graphene and graphene oxide nanowalls against bacteria, ACS Nano 4 (10) (2010) 5731–5736.

[27] W.B. Hu, C. Peng, W.J. Luo, M. Lv, X.M. Li, D. Li, Q. Huang, C.H. Fan, Graphene-based antibacterial paper, ACS Nano 4 (7) (2010) 4317–4323.

[28] H. Hong, K. Yang, Y. Zhang, J.W. Engle, L.Z. Feng, Y.A. Yang, T.R. Nayak, S. Goel, J. Bean, C.P. Theuer, T.E. Barnhart, Z. Liu, W.B. Cai, In vivo targeting and imaging of tumor vasculature with radiolabeled, antibody-conjugated nanographene, ACS Nano 6 (3) (2012) 2361–2370.

[29] H.J. Zhou, B. Zhang, J.J. Zheng, M.F. Yu, T. Zhou, K. Zhao, Y.X. Jia, X.F. Gao, C.Y. Chen, T.T. Wei, The inhibition of migration and invasion of cancer cells by graphene via the impairment of mitochondrial respiration, Biomaterials 35 (5) (2014) 1597–1607.

[30] S.Y. Yin, Y.L. Wu, B.H. Hu, Y. Wang, P.Q. Cai, C.K. Tan, D.P. Qi, L.Y. Zheng, W.R. Leow, N.S. Tan, S.T. Wang, X.D. Chen, Three-dimensional graphene composite macroscopic structures for capture of cancer cells, Adv. Mater. Interfaces 1 (1) (2014) 1300043.

[31] M. Lv, Y.J. Zhang, L. Liang, M. Wei, W.B. Hu, X.M. Li, Q. Huang, Effect of graphene oxide on undifferentiated and retinoic acid-differentiated SH-SY5Y cells line, Nanoscale 4 (13) (2012) 3861–3866.

[32] K.H. Liao, Y.S. Lin, C.W. Macosko, C.L. Haynes, Cytotoxicity of graphene oxide and graphene in human erythrocytes and skin fibroblasts, ACS Appl. Mater. Interfaces 3 (7) (2011) 2607–2615.

[33] O. Akhavan, E. Ghaderi, A. Akhavan, Size-dependent genotoxicity of graphene nanoplatelets in human stem cells, Biomaterials 33 (32) (2012) 8017–8025.

[34] O. Akhavan, E. Ghaderi, H. Emamy, F. Akhavan, Genotoxicity of graphene nanoribbons in human mesenchymal stem cells, Carbon 54 (2013) 419–431.

[35] O. Akhavan, E. Ghaderi, A. Esfandiar, Wrapping Bacteria by Graphene Nanosheets for Isolation from Environment, Reactivation by Sonication, and Inactivation by Near-Infrared Irradiation, J. Phys. Chem. B 115 (19) (2011) 6279–6288.

[36] O. Akhavan, E. Ghaderi, Escherichia coli bacteria reduce graphene oxide to bactericidal graphene in a self-limiting manner, Carbon 50 (5) (2012) 1853–1860.

[37] O.N. Ruiz, K.A.S. Fernando, B.J. Wang, N.A. Brown, P.G. Luo, N.D. McNamara, M. Vangsness, Y.P. Sun, C.E. Bunker, Graphene oxide: a nonspecific enhancer of cellular growth, ACS Nano 5 (10) (2011) 8100–8107.

[38] H.Q. Chen, D. Gao, B. Wang, R.F. Zhao, M. Guan, L.N. Zheng, X.Y. Zhou, Z.F. Chai, W.Y. Feng, Graphene oxide as an anaerobic membrane scaffold for the enhancement of B. adolescentis proliferation and antagonistic effects against pathogens E-coli and S-aureus, Nanotechnology 25 (16) (2014) 165101.

[39] D. Wang, G.W. Wang, G.Q. Zhang, X.C. Xu, F.L. Yang, Using graphene oxide to enhance the activity of anammox bacteria for nitrogen removal, Bioresour. Technol. 131 (2013) 527–530.

[40] J. Tang, Q. Chen, L.G. Xu, S. Zhang, L.Z. Feng, L. Cheng, H. Xu, Z. Liu, R. Peng, Graphene oxide-silver nanocomposite as a highly effective antibacterial agent with species-specific mechanisms, ACS Appl. Mater. Interfaces 5 (9) (2013) 3867–3874.

[41] T.F. Tian, X.Z. Shi, L. Cheng, Y.C. Luo, Z.L. Dong, H. Gong, L.G. Xu, Z.T. Zhong, R. Peng, Z. Liu, Graphene-based nanocomposite as an effective, multifunctional, and recyclable antibacterial agent, ACS Appl. Mater. Interfaces 6 (11) (2014) 8542–8548.

[42] K. Yang, S.A. Zhang, G.X. Zhang, X.M. Sun, S.T. Lee, Z. Liu, Graphene in mice: ultrahigh in vivo tumor uptake and efficient photothermal therapy, Nano Lett. 10 (9) (2010) 3318–3323.

[43] G. Fu, T. Huang, J. Buss, C. Coltharp, Z. Hensel, J. Xiao, In vivo structure of the E. Coli ftsz-ring revealed by photoactivated localization microscopy (PALM), Biophys. J. 100 (3) (2011) 615.

[44] Y.Y. Zhao, C.J. Ye, W.W. Liu, R. Chen, X.Y. Jiang, Tuning the composition of aupt bimetallic nanoparticles for antibacterial application, Angew. Chem. Int. Ed. 53 (31) (2014) 8127–8131.

[45] J. Azeredo, V. Lazarova, R. Oliveira, Methods to extract the exopolymeric matrix from biofilms: a comparative study, Water Sci. Technol. 39 (7) (1999) 243–250.

[46] M. Dubois, K.A. Gilles, J.K. Hamilton, P.A. Rebers, F. Smith, Colorimetric Method for Determination of Sugars and Related Substances, Anal. Chem. 28 (3) (1956) 350–356.

[47] M.M. Bradford, A rapid and sensitive method for the quantitation of microgram quantities of protein, Anal. Biochem. 72 (1–2) (1976) 248–254.

[48] J. Buss, C. Coltharp, J. Xiao, Super-resolution imaging of the bacterial division machinery, Jove-J Vis. Exp. 71 (2013) e50048.

[49] D.J. Ferullo, D.L. Cooper, H.R. Moore, S.T. Lovett, Cell cycle synchronization of Escherichia coli using the stringent response, with fluorescence labeling assays for DNA content and replication, Methods 48 (1) (2009) 8–13.

[50] Z.P. Wang, L.L. Liu, H. Yao, W.M. Cai, Effects of extracellular polymeric substances on aerobic granulation in sequencing batch reactors, Chemosphere 63 (10) (2006) 1728–1735.

[51] A.M. Romani, K. Fund, J. Artigas, T. Schwartz, S. Sabater, U. Obst, Relevance of polymeric matrix enzymes during biofilm formation, Microb. Ecol. 56 (3) (2008) 427–436.

[52] H. Zeng, S. Zhang, K.Y. Yang, T. Wang, J.L. Hu, L.L. Huang, G. Wu, Knockdown of second mitochondria-derived activator of caspase expression by rnai enhances growth and cisplatin resistance of human lung cancer cells, Cancer Biother. Radiopharm. 25 (6) (2010) 705–712.

[53] J.K.C. Ma, P.M.W. Drake, P. Christou, The production of recombinant pharmaceutical proteins in plants, Nat. Rev. Genet. 4 (10) (2003) 794–805.

[54] E. Hochuli, W. Bannwarth, H. Dobeli, R. Gentz, D. Stuber, Genetic approach to facilitate purification of recombinant proteins with a novel metal chelate adsorbent, Bio-Technol 6 (11) (1988) 1321–1325.
[55] J. Courcelle, P.C. Hanawalt, Participation of recombination proteins in rescue of arrested replication forks in UV-irradiated Escherichia coli need not involve recombination, Proc. Natl. Acad. Sci. U. S. A. 98 (15) (2001) 8196–8202.
[56] R. Vincentelli, C. Bignon, A. Gruez, S. Canaan, G. Sulzenbacher, M. Tegoni, V. Campanacci, C. Cambillau, Medium-scale structural genomics: strategies for protein expression and crystallization, Accounts Chem. Res. 36 (3) (2003) 165–172.
[57] X.F. Liu, L. Liu, Y.G. Wang, X.L. Wang, Y.L. Ma, Y.C. Li, The Study on the factors affecting transformation efficiency of E-coli competent cells, Pak J. Pharm. Sci. 27 (3) (2014) 679–684.
[58] C. Rutschmann, S. Baumann, J. Cabalzar, K.B. Luther, T. Hennet, Recombinant expression of hydroxylated human collagen in Escherichia coli, Appl. Microbiol. Biotechnol. 98 (10) (2014) 4445–4455.
[59] O. Akhavan, E. Ghaderi, H. Emamy, Nontoxic concentrations of PEGylated graphene nanoribbons for selective cancer cell imaging and photothermal therapy, J. Mater. Chem. 22 (38) (2012) 20626–20633.
[60] X.Q. Guo, N. Mei, Assessment of the toxic potential of graphene family nanomaterials, J. Food Drug Anal. 22 (1) (2014) 105–115.